Proc. Natl. Acad. Sci. USA
Vol. 95, pp. 12083–12087, October 1998
Applied Physical Sciences

A peptide that inhibits hydroxyapatite growth is in an extended conformation on the crystal surface

JOANNA R. LONG[†], JOHN L. DINDOT[‡], HENRY ZEBROSKI[‡], SUZANNE KIIHNE[‡], RUTILIO H. CLARK[†], ALLISON A. CAMPBELL[§], PATRICK S. STAYTON[†¶], AND GARY P. DROBNY[‡‖]

Departments of [†]Bioengineering and [‡]Chemistry, University of Washington, Seattle, WA 98195; and [§]Pacific Northwest National Laboratory, Richland, WA 99352

Communicated by Alexander Pines, University of California, Berkeley, CA, July 30, 1998 (received for review February 3, 1998)

ABSTRACT **Proteins play an important role in the biological mechanisms controlling hard tissue development, but the details of molecular recognition at inorganic crystal interfaces remain poorly characterized. We have applied a recently developed homonuclear dipolar recoupling solid-state NMR technique, dipolar recoupling with a windowless sequence (DRAWS), to directly probe the conformation of an acidic peptide adsorbed to hydroxyapatite (HAP) crystals. The phosphorylated hexapeptide, DpSpSEEK (N6, where pS denotes phosphorylated serine), was derived from the N terminus of the salivary protein statherin. Constant-composition kinetic characterization demonstrated that, like the native statherin, this peptide inhibits the growth of HAP seed crystals when preadsorbed to the crystal surface. The DRAWS technique was used to measure the internuclear distance between two ^{13}C labels at the carbonyl positions of the adjacent phosphoserine residues. Dipolar dephasing measured at short mixing times yielded a mean separation distance of 3.2 ± 0.1 Å. Data obtained by using longer mixing times suggest a broad distribution of conformations about this average distance. Using a more complex model with discrete α-helical and extended conformations did not yield a better fit to the data and was not consistent with chemical shift analysis. These results suggest that the peptide is predominantly in an extended conformation rather than an α-helical state on the HAP surface. Solid-state NMR approaches can thus be used to determine directly the conformation of biologically relevant peptides on HAP surfaces. A better understanding of peptide and protein conformation on biomineral surfaces may provide design principles useful for the modification of orthopedic and dental implants with coatings and biological growth factors that are designed to enhance biocompatibility with surrounding tissue.**

The biological mechanisms that control hard tissue construction have attracted a great deal of recent attention in fields ranging from biology and chemistry to materials science and bioengineering (1, 2). A better understanding of the biomolecular mechanisms used to promote bone and tooth growth could provide important design principles for the development of biocompatible implant materials. Increasing interest is also being paid to nature's processing strategies by materials scientists looking for bio-inspired methods to engineer unique ceramics coatings or composites for use in magnetic, optical, biomedical, and protective coatings applications. The crystal engineering capabilities of proteins play an important role in many of these biomineralization processes. An important class of proteins directly involved in biomineralization is the non-collagenous, acidic proteins found in bone tissue, salivary fluids, and urinary compartments. Key examples are osteocalcin, osteonectin, bone sialoprotein, and osteopontin from bone tissues, and the proline-rich acidic proteins such as statherin found in salivary fluids (3–9). Considerable insight has been gained into these proteins' functional activities, and their ability to control crystallite growth processes, orientation, and morphology is well documented. Similarly remarkable crystal engineering properties have been documented in marine organisms, where soluble proteins have been shown to control crystal phase switching and to regulate the growth of specific crystal faces (10–16). Little is known, however, of the detailed structure–function relationships used by such proteins to mediate hard-tissue growth processes.

Statherin, a small protein isolated from salivary compartments, functions as an effective inhibitor of hydroxyapatite (HAP) primary and secondary crystallization (17, 18). The statherin primary amino acid sequence is characterized by a negatively charged N terminus consisting of a DSSEEK sequence, and the serines are post-translationally phosphorylated (19). There is no direct three-dimensional structure information available for statherin, but secondary structure predictions suggest that the N terminus has a propensity for α-helix formation, and circular dichroism studies demonstrate the presence of some α-helical conformation in solution (20, 21). The existence of secondary structure in other acidic proteins has also been predicted and hypothesized to play a role in crystal recognition through lattice-matching mechanisms (22–24). As initially demonstrated by Hay, Nancollas, and coworkers, peptides from this N terminus of statherin bind effectively to HAP seed crystals and inhibit their further growth in metastable supersaturated solutions (25, 26).

Solid-state NMR has yielded important insight into the structure and dynamics of biomolecules in mesogenic or amorphous solids where x-ray crystallographic approaches are not applicable (27–33). Cross-polarization with magic-angle spinning (CPMAS) and dipolar recoupling experiments provide an opportunity to characterize biomolecular structure at solid surfaces of relevance to biology and to the many existing and developing technologies that use immobilized biomolecules. We report here an initial solid-state NMR study that uses the recently developed dipolar recoupling solid-state NMR technique, dipolar recoupling with a windowless sequence (DRAWS) (34), to directly probe the conformation of an acidic N-terminal peptide from statherin on the surface of HAP crystals. This N-terminal statherin peptide binds tightly to HAP crystals and strongly modulates the secondary nucleation and crystal growth rates in analogous fashion to the parent protein.

Abbreviations: HAP, hydroxyapatite; DRAWS, Dipolar Recoupling with a Windowless Sequence; N6, the N-terminal hexapeptide of statherin; CPMAS, cross-polarization with magic-angle spinning.

[¶]To whom reprint requests may be addressed at: Department of Bioengineering, Box 357962, University of Washington, Seattle, WA 98195. e-mail: stayton@bioeng.washington.edu.
[‖]To whom reprint requests may be addressed at: Department of Chemistry, Box 351700, University of Washington, Seattle, WA 98195. e-mail: drobny@macmail.chem.washington.edu.

The publication costs of this article were defrayed in part by page charge payment. This article must therefore be hereby marked "*advertisement*" in accordance with 18 U.S.C. §1734 solely to indicate this fact.

MATERIALS AND METHODS

Materials. Protected amino acids and fluorenylmethoxycarbonyl-lysine-(*t*-butoxycarbonyl) resin were purchased from NovaBiochem. Carbonyl ^{13}C-labeled serine was purchased from Cambridge Isotope Laboratories (Cambridge, MA). Crystalline HAP was purchased from Clarkson Chromatography Products (South Williamsport, PA).

Peptide Synthesis and Characterization. The N-terminal hexapeptide of statherin (N6), DSSEEK, was synthesized by standard fluorenylmethoxycarbonyl procedures by using fluorenylmethoxycarbonyl-lysine-(*t*-butoxycarbonyl) Wang resin (substitution 0.4 mmol/g) on an automated Applied Biosystems 433A peptide synthesizer. Carbonyl ^{13}C-labeled serine was protected by using 9-fluoroenylmethyl succinimidyl carbonate before incorporation into the peptide. The peptide was phosphorylated by using di-*tert*-butyl-*N*,*N*-diisopropylphosphoramidite, followed by oxidation with 80% *t*-butylhydroperoxide to yield the *t*-butyl-protected phosphate moiety. The phosphopeptide was then cleaved from the resin by using a standard trifluoroacetic acid cleavage cocktail, purified to homogeneity by HPLC, and verified by mass spectrometry. Circular dichroism analysis of N6 was conducted on a model 62A DS circular dichroism spectrometer (Aviv Associates, Lakewood, NJ) at 25°C. Spectra were collected in a 4-ml cuvette at 60 rpm with 26 μM N6 peptide in 10 mM NaCl/2.5 mM potassium phosphate buffer, pH 7.5, and then under the same conditions with $CaCl_2$ at 0.4, 2.0, or 8.0 mM.

Peptide Adsorption to HAP. HAP was characterized by x-ray powder diffraction to confirm the absence of other calcium phosphate phases. Crystal-specific surface area was determined to be 63 m^2/g by using N_2 Brunauer-Emmett-Teller measurements. Phosphopeptide was physisorbed to HAP by dissolving an excess of peptide in a saturated HAP solution containing a suspension of 100 mg of HAP crystallites buffered to pH 7.5. After 4 h of equilibration, the HAP crystallites were separated from the peptide in solution by centrifugation and were washed repeatedly with buffered saturated HAP solution. NMR samples were subsequently lyophilized.

Constant-Composition Kinetics. Supersaturated HAP solutions at pH 7.4 and ionic strength of 0.01 mol/liter were prepared in glass vessels at 25°C. Nitrogen gas, saturated with respect to the background electrolyte, was continuously bubbled through the solution to exclude carbon dioxide. The solution pH was measured by using a pH electrode (Corning) and Radiometer (Copenhagen) pH meter. Metastable supersaturated HAP solutions were prepared by the slow addition of stock solutions with constant stirring to minimize local regions of high concentrations. Triply distilled, deionized water was added to the reaction vessel first, followed by the addition of the background electrolyte (NaCl, final concentration 0.01 M), KH_2PO_4 (final concentration 4.50×10^{-4} M), and $CaCl_2$ (final concentration 2.69×10^{-4} M) solutions, respectively. The pH was adjusted to the final value by the slow addition of KOH. On reaching a stable pH, the potentiostat (Radiometer) was set to the desired pH. Crystal growth was initiated by the addition of seed HAP crystals to the supersaturated solution. For experiments with adsorbed protein, pretreated crystallites were added to the reaction vessel in the form of a suspension (0.01 M NaCl). On introduction of seed crystals, the onset of growth resulted in a decrease in calcium ions in solution, triggering the potentiostat to simultaneously add titrant solutions to the supersaturated solution, thereby restoring the lattice ion activities to their preset value. The preparation of titrant solutions took into account both lattice depletion due to crystal growth and dilution effects caused by the addition of multiple titrants. Typically, lattice ion concentrations were maintained to within approximately 2% of their original value, thus keeping the solution supersaturation constant throughout the duration of the experiment. To verify supersaturation consistency, aliquots were periodically withdrawn from the reaction mixture, filtered, and analyzed for calcium (atomic absorption) and phosphate (UV) ion concentrations.

Solid-State NMR Studies. Solid-state NMR experiments were carried out on a home-built spectrometer operating at a ^{13}C NMR frequency of 100.7 MHz by using a Doty Scientific (Columbia, SC) triply resonant magic-angle spinning probe. CPMAS experiments used a 5-μsec ^1H 90° pulse and a 2-msec mixing time. The chemical shifts were referenced relative to crystalline [1,4-^{13}C] succinic acid and converted to a tetramethylsilane reference by the addition of 179 ppm. The DRAWS pulse sequence is shown in Fig. 1 and consists of a series of pulses applied in synchrony with the rotor cycle. The 90° pulses prevent the dipolar interaction from being averaged during magic-angle spinning while the 360° pulses serve to suppress chemical shift interactions. The transverse magnetization is then observed stroboscopically every four rotor cycles and normalized with respect to the magnetization observed without any mixing. A ^{13}C rf field of 38.5 kHz, corresponding to a 6.5-μsec $\pi/2$ pulse, was used during the DRAWS mixing period, and proton decoupling of >125 kHz was applied throughout the DRAWS and acquisition periods. The sample was spun at 4525 ± 5 Hz in agreement with the 221-μsec DRAWS cycle time. The DRAWS experiment was run in triplicate by using 2048 scans per spectrum and a repetition time of 5 sec. Samples consisted of approximately 2 mg of phosphopeptide adsorbed to 100 mg of HAP packed into a 5-mm rotor. The DRAWS data were obtained both on a doubly (Dp*Sp*SEEK) and a singly ^{13}C-carbonyl-labeled sample (Dp*SpSEEK) to determine the relevant relaxation parameters. Simulated DRAWS decay curves were calculated by using numerical methods that incorporated the observed relaxation and chemical shift anisotropies.

RESULTS

Peptide Characterization. Solid-phase synthesis with subsequent phosphorylation produced DpSpSEEK (N6) in high yield, as verified by electrospray mass spectrometry (molecular weight = 856.6, theoretical molecular weight = 855.6). Circular dichroism analysis verified that unadsorbed N6 exists as a random coil in buffered solution in the presence or absence of calcium ions (data not shown).

Effect of N6 on Secondary HAP Growth. Constant-composition kinetic methods comparing the growth rate of the HAP seed crystals in the presence and absence of preadsorbed N6 indicated that the peptide inhibits crystallization >99% relative to the uncoated control. These results are consistent

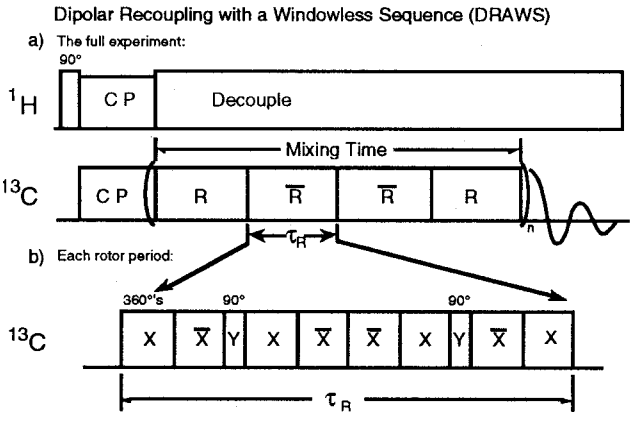

FIG. 1. Dipolar recoupling with a windowless sequence (DRAWS). The complete sequence with a four-rotor supercycle is shown in *a*. In *b*, the basic sequence over one rotor cycle is shown.

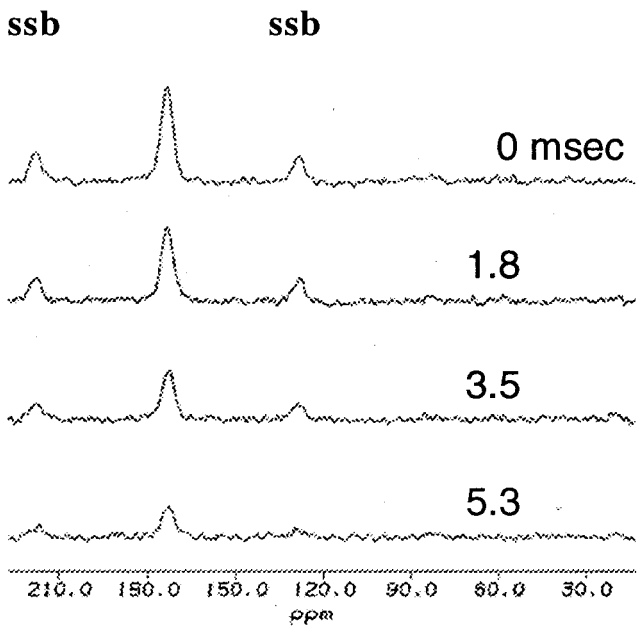

FIG. 2. CPMAS and DRAWS spectra of Dp*Sp*SEEK showing relative intensity at the indicated mixing times. ssb, spinning sidebands.

with those reported for N-terminal penta- and hexapeptides of statherin (25, 26).

Characterization of N6 Conformation by Solid-State NMR. The average chemical shift of the phosphoserine carbonyl carbons in Dp*Sp*SEEK, both neat and adsorbed to HAP, is 173 ppm (Fig. 2), and the carbonyl resonances show considerable dispersion ($\Delta\nu_{1/2} > 4$ ppm). Chemical shift spectra of crystalline peptides acquired under identical conditions typically show linewidths on the order of 0.5–1 ppm. This broadening is probably because of structural inhomogeneity in the peptide rather than relaxation (based on the measured T_{2SQ} value of 10 msec) or spectral overlap (the same breadth was seen in both doubly and singly labeled samples). Variation of the backbone torsion angles can lead to changes in carbonyl chemical shifts of up to 7 ppm. Comparison of observed DRAWS dephasing with simulated curves provides additional evidence of this interpretation (Fig. 3). The calculated curves for α-helix ($\phi = -60$, 3.0 Å, 270 Hz dipolar coupling), β-sheet ($\phi = -120$ or -140, 3.4 or 3.5 Å, 200 or 180 Hz), and fully extended ($\phi = -180$, 3.7 Å, 150 Hz) conformations clearly show poor agreement with the experimental data. A dephasing curve calculated assuming a single secondary structure (phi = -90, 3.2 Å, 240 Hz) shows good agreement with the initial decay observed experimentally, but does not model the long-time behavior well. Experiments run on a sample consisting of 20% doubly labeled peptide mixed with 80% natural abundance peptide before adsorption showed identical results (data not shown), ruling out the possibility of intermolecular interactions. Simulations performed assuming an even distribution of conformations over all reasonable values of ϕ (-30 to -180) show better agreement. Additionally, a model generated assuming 60% β-sheet and 40% α-helix shows good agreement. However, no splitting is evident in the chemical shift spectrum, so a broad Gaussian or even distribution of conformers is more likely. Peptide backbone dynamics are

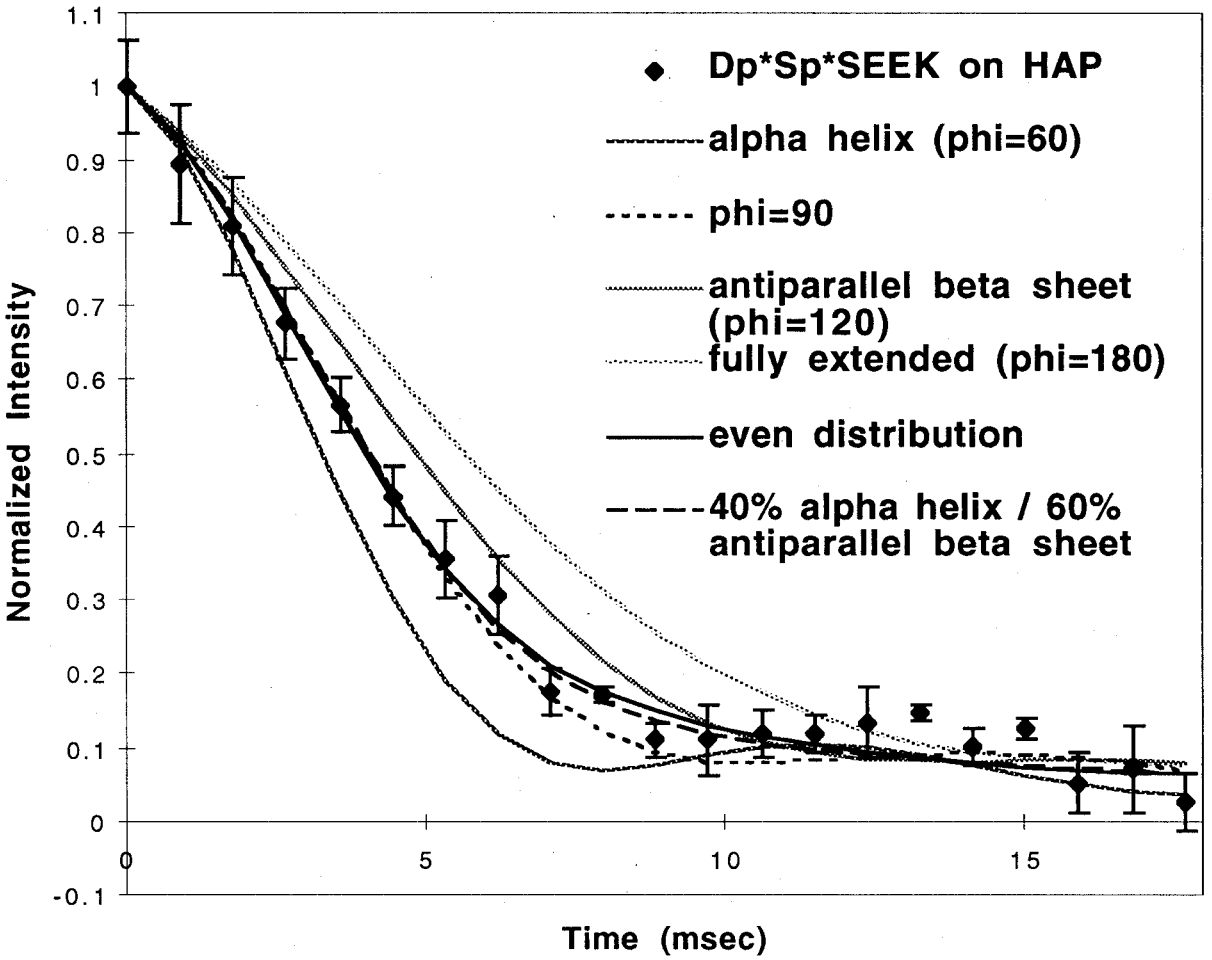

FIG. 3. DRAWS dephasing curve observed for Dp*Sp*SEEK. The experimental data are shown, along with simulations discussed in the text.

likely to be insignificant, since the samples are lyophilized and adsorption of peptides to hydroxyapatite has been shown to further restrict backbone motions (27).

DISCUSSION

We report here a determination of the conformation of a phosphorylated peptide on the HAP crystal surface by using CPMAS and DRAWS solid-state NMR techniques. Chemical shift measurements provide a useful means of determining gross structural features. Asakura *et al.* used serine to distinguish between α-helical (silk I, carbonyl carbon resonance at 173.7 ppm) and β-sheet (silk II, 172.3 ppm) conformations in silk (28). However, phosphorylation of the serines in N6 and adsorption to a highly ionic surface could significantly alter the chemical shift of the carbonyls and/or increase the range of chemical shifts observed. It is interesting to note that the average chemical shift (173 ppm) of N6 is intermediate to those observed in the two forms of silk. This agrees well with the average distance of 3.2 Å measured by using DRAWS, corresponding to a ϕ angle midway between the α-helical and β-sheet conformations. The breadth of the carbonyl resonance, however, indicates that the range of possible backbone torsional angles and/or interactions of the carbonyls with the surface is quite broad. Direct distance measurements provide a means of more accurate interpretation.

To obtain high-resolution, solid-state NMR spectra of rare spin 1/2 nuclei, magic-angle spinning is applied to remove chemical shift anisotropies. However, this technique also attenuates dipolar interactions. This averaging of the dipole interactions may be counteracted by introducing 180° or 90° pulses appropriately synchronized with the spinning of the sample. DRAWS is a homonuclear dipolar recoupling technique capable of measuring distances between spin 1/2 nuclei, irrespective of their isotropic chemical shift separation or chemical shift anisotropy (35). DRAWS is ideally suited to measuring individual torsional angles in peptide systems. Measuring distances between successive carbonyl carbons allows direct determination of the torsion angle phi. Although the carbonyl chemical shift anisotropies are considerably larger than the dipolar couplings and typically have degenerate isotropic chemical shifts, DRAWS is insensitive to either of these factors. DRAWS may also be used for measuring distances between nuclei with large isotropic shift differences. Because DRAWS is insensitive to both chemical shift dispersion and the relative orientations of the chemical shift anisotropies, it is well suited to studying systems that contain an ensemble of conformations instead of crystalline regularity, since the dipolar recoupling efficiency is independent of any correlation between the chemical shifts in a given sample. This characteristic is especially useful in peptides, since the correlation of the carbonyl chemical shifts to secondary structure is opposite in sign to that of the alpha and beta carbons.

The N-terminal hexapeptide of salivary statherin displays a random coil conformation in solution, as determined from circular dichroism studies, but it significantly affects the crystallization of HAP. However, it does not adopt a single secondary structure on adsorption to achieve this. When adsorbed on HAP seed crystals, this peptide also shows little structural regularity, as directly determined by solid-state NMR. The DRAWS experiment yielded an internuclear distance of 3.2 Å between the two ^{13}C-labeled serine carbonyls in the peptide adsorbed to HAP crystals and determined that significant conformational heterogeneity exists.

Additional studies are being done on the N-terminal 15 amino acid fragment of statherin, which shows considerable helical content in solution (36), to determine whether it retains significant amounts of secondary structure on adsorption to the HAP surface. The determination of peptide molecular conformation *in situ* on biomineral surfaces should provide important insight into the molecular recognition mechanisms used in biomineralization. These solid-state NMR approaches should also prove valuable in the design and characterization of molecules that inhibit dystrophic calcification, promote biocompatibility in biomaterial or tissue engineering settings, or are used in diagnostic and biosensor technologies.

We gratefully acknowledge the support of the National Institute of Dental Research (DE 12554–01), the National Science Foundation (EEC-9529161 and DMR-9616212), and the Department of Energy (DE-AC06–76RL01830).

1. Weiner, S. & Addadi, L. (1997) *J. Mater. Chem.* **7,** 689–702.
2. Stupp, S. I. & Braun, P. V. (1997) *Science.* **277,** 1242–1248.
3. George, A., Sabsay, B., Simonian, P. A. & Veis, A. (1993) *J. Biol. Chem.* **268,** 12624–12630.
4. Goldberg, H. A., Warner, K. J., Stillman, M. J. & Hunter, G. K. (1996) *Connect. Tissue Res.* **35,** 385–392.
5. Hunter, G. K., Hauschka, P. V., Poole, A. R., Rosenberg, L. C. & Goldberg, H. A. (1996) *Biochem. J.* **317,** 59–64.
6. Hunter, G. K. & Goldberg, H. A. (1994) *Biochem. J.* **302,** 175–179.
7. Kestell, M. F., Sekijima, J., Lee, S. P., Park, H. Z., Long, M. & Kaler, E. W. (1992) *Hepatology* **16,** 1315–1321.
8. Fujisawa, R., Wada, Y., Nodasaka, Y. & Kuboki, Y. (1996) *Biochim. Biophys. Acta* **1292,** 53–60.
9. Johnsson, M., Levine, M. J. & Nancollas, G. H. (1993) *Crit. Rev. Oral Biol. Med.* **4,** 371–378.
10. Aizenberg, J., Hanson, J., Koetzle, T. F., Weiner, S. & Addadi, L. (1997) *J. Am. Chem. Soc.* **119,** 881–886.
11. Belcher, A. M., Wu, X. H., Christensen, R. J., Nahsma, P. K., Stucky, G. D. & Morse, D. E. (1996) *Nature (London)* **381,** 56–58.
12. Berman, A., Addadi, L. & Weiner, S. (1988) *Nature (London)* **331,** 546–548.
13. Berman, A., Hanson, J., Leiserowitz, L., Koetzle, T. F., Weiner, S. & Addadi, L. (1993) *Science* **259,** 776–779.
14. Falini, G., Albeck, S., Weiner, S. & Addadi, L. (1996) *Science* **271,** 67–69.
15. Hanein, D., Geiger, B. & Addadi, L. (1994) *Science* **263,** 1413–1416.
16. Walters, D. A., Smith, B. L., Belcher, A. M., Paloczi, G. T., Stucky, G. D., Morse, D. E. & Hansma, P. K. (1997) *Biophys. J.* **72,** 1425–1433.
17. Hay, D. I., Smith, D. J., Schluckebier, S. K. & Moreno, E. C. (1984) *J. Dent. Res.* **63,** 857–863.
18. Moreno, E. C., Varughese, K. & Hay, D. I. (1979) *Calcif. Tissue Int.* **28,** 7–16.
19. Schlesinger, D. H. & Hay, D. I. (1977) *J. Biol. Chem.* **252,** 1689–1695.
20. Douglas, W. H., Reeh, E. S., Ramasubbu, N., Raj, P. A., Bhandry, K. K. & Levine, M. J. (1991) *Biochem. Biophys. Res. Commun.* **180,** 91–97.
21. Gururaja, T. L. & Levine, M. J. (1996) *Pept. Res.* **9,** 283–289.
22. Sicheri, F. & Yang, D. S. C. (1995) *Nature (London)* **375,** 427–431.
23. DeOliviera, D. B. (1997) *J. Am. Chem. Soc.* **119,** 10627–10631.
24. Hauschka, P. V. & Carr, S. A. (1982) *Biochemistry* **21,** 2538–2547.
25. Schwartz, S. S., Hay, D. I. & Schluckebier, S. K. (1992) *Calcif. Tissue Int.* **50,** 511–517.
26. Wikiel, K., Burke, E. M., Perich, J. W., Reynolds, E. C. & Nancollas, G. H. (1994) *Arch. Oral Biol.* **39,** 715–721.
27. Fernandez, V. L., Reimer, J. A. & Denn, M. M. (1992) *J. Am. Chem. Soc.* **114,** 9634–9642.
28. Asakura, T., Demura, M., Date, T., Miyashita, N., Ogawa, K. & Williamson, M. P. (1997) *Biopolymers* **41,** 193–203.
29. Heller, J., Kolbert, A. C., Larsen, R., Ernst, M., Bekker, T., Baldwin, M., Prusiner, S. B., Pines, A. & Wemmer, D. E. (1996) *Protein Sci.* **5,** 1655–1661.
30. Klug, C. A., Burzio, L. A., Waite, J. H. & Schaefer, J. (1996) *Arch. Biochem. Biophys.* **333,** 221–224.
31. Lansbury, P. T., Costa, P. R., Griffiths, J. M., Simon, E. J., Auger, M., Halverson, K. J., Kocisko, D. A., Hendsh, Z. S.,

Ashburn, T. T., Spencer, R. G. S., *et al.* (1995) *Nat. Struct. Biol.* **2,** 990–998.
32. Merritt, M. E., Christensen, A. M., Kramer, K. J., Hopkins, T. L. & Schaefer, J. (1996) *J. Am. Chem. Soc.* **118,** 11278–11282.
33. Simmons, A. H., Michal, C. A. & Jelinski, L. W. (1996) *Science* **271,** 84–87.
34. Gregory, D. M., Mitchell, D. J., Stringer, J. A., Kiihne, S., Shiels, J. C., Callahan, J., Mehta, M. A. & Drobny, G. P. (1995) *Chem. Phys. Lett.* **246,** 654–663.
35. Mehta, M. A., Gregory, D. M., Kiihne, S., Mitchell, D. J., Hatcher, M. E., Shiels, J. C. & Drobny, G. P. (1996) *Solid State Nucl. Magn. Reson.* **7,** 211–228.
36. Raj, P. A., Johnsson, M., Levine, M. J. & Nancollas, G. H. (1992) *J. Biol. Chem.* **267,** 5968–5976.